Available online at www.sciencedirect.com
ScienceDirect
International Journal of Non-Linear Mechanics 43 (2008) 345–365
INTERNATIONAL JOURNAL OF NON-LINEAR MECHANICS
www.elsevier.com/locate/nlm

Non-linear buckling and postbuckling behavior of thin-walled beams considering shear deformation

Sebastián P. Machado*

Grupo Análisis de Sistemas Mecánicos, Facultad Regional Bahía Blanca, Universidad Tecnológica Nacional, 11de abril 461, B8000LMI Bahía Blanca, Argentina

Received 20 April 2007; received in revised form 28 November 2007; accepted 21 December 2007

Abstract

The static stability of thin-walled composite beams, considering shear deformation and geometrical non-linear coupling, subjected to transverse external force has been investigated in this paper. The theory is formulated in the context of large displacements and rotations, through the adoption of a shear deformable displacement field (accounting for bending and warping shear) considering moderate bending rotations and large twist. This non-linear formulation is used for analyzing the prebuckling and postbuckling behavior of simply supported, cantilever and fixed-end beams subjected to different load condition. Ritz's method is applied in order to discretize the non-linear differential system and the resultant algebraic equations are solved by means of an incremental Newton–Rapshon method. The numerical results show that the beam loses its stability through a stable symmetric bifurcation point and the postbuckling strength is in relation with the buckling load value. Classical predictions of lateral buckling are conservative when the prebuckling displacements are not negligible and the non-linear buckling analysis is required for reliable solutions. The analysis is supplemented by investigating the effects of the variation of load height parameter. In addition, the critical load values and postbuckling response obtained with the present beam model are compared with the results obtained with a shell finite element model (Abaqus).

Keywords: Thin-walled beams; Shear flexibility; Ritz method; Postbuckling; Prebuckling

1. Introduction

Thin-walled beams of open and closed cross-section are widely used as structural elements within the fields of civil, aerospace and mechanical engineering, offering a high performance in terms of minimum weight for a given strength. These kinds of members are often designed to work under postbuckling conditions. It is well known that the spatial buckling behavior of thin-walled beam structures is very complex due to the coupling effect of extensional, bending and torsional deformation. Besides, such flexible structures can undergo large displacements and rotations without exceeding their elastic limits. Therefore, a non-linear theory is required for the accurate behavior prediction of such structures. For example, the limitation of the linear buckling analysis of beam problems [1] is the omission of any consideration of the effect of prebuckling deflections of the beam. This omission may be sufficiently accurate when the prebuckling deflection of the beam is negligible. In other cases, however, the effect of the prebuckling deflections must be taken into account to obtain accurate predictions of buckling loads. In particular, lateral buckling is a relevant phenomenon that involves mechanical complications, since structures may experience large or moderately large deflections and rotations before buckling occurs. Moreover, the linear buckling gives no information about the shape of the secondary path of equilibrium (postbuckling). Sometimes the behavior of a structure can be understood only if the shape of the secondary path is known. Thus, the additional load-carrying capacity after buckling can be determined. For this reason, knowledge of the postbuckling response and the ultimate load of such structures are essential for designers. In particular, this knowledge will allow beams to be designed efficiently and economically to fully exploiting their postbuckling strength.

* Tel.: +54 0291 4555220; fax: +54 0291 4555311.
E-mail address: smachado@frbb.utn.edu.ar

0020-7462/$ - see front matter © 2008 Elsevier Ltd. All rights reserved.
doi:10.1016/j.ijnonlinmec.2007.12.019

To understand the behaviors of such flexible structures and to evaluate their elastic limits many different formulations and numerical procedures for the buckling and postbuckling analysis of beams have been proposed. Euler in 1744 [2] was one of the first in investigating the elastic flexural postbuckling behavior of columns, by using the exact expression for curvature instead of the small deflection approximation. This resulted in a postbuckling curve that rises so slowly that there is not significant increase in the load-carrying capacity until the deformations increase considerably. The buckling and postbuckling analysis of thin-walled beams has been the subject of considerable research. Among the first works carried out for thin-walled beams, Barsoum and Gallagher [3] studied the torsional and flexural–torsional stability of a bi-symmetric I-beam subjected to conservative loads. Woolcock and Trahair [4] carried out theoretical and experimental studies on the postcritical behavior of thin-walled I-beams for different boundary conditions.

Since, in general, exact solutions cannot be obtained or are tedious and time consuming, the only recourse is to resort to approximate postbuckling analyses. There are several studies based on the finite element method, Bazant and Nimeiri [5] developed a general stiffness analysis of spatial large deflections and postbuckling behavior of thin-walled members of asymmetric open cross-section. Bathe and Bolourchi [6], Yang and McGuire [7], Hasegawa et al. [8], Kitipornchai et al. [9] and Chen and Blandford [10] carried out studies of large deflections in beams using an updated Lagrangian procedure. A consistent co-rotational total Lagrangian formulation was presented by Hsiao and Lin [11–13] in the geometrically non-linear analysis of mono- and bi-symmetric beams. In their formulation they considered third-order terms of the nodal forces, corresponding to the torsional twist. Through the different models used, they showed the influence of the third-order terms on the buckling and postbuckling behavior of 3-D beams.

Grimaldi and Pignataro [14] studied the initial postbuckling behavior of beams subjected to an axial load, using a perturbation technique based on Koiter's method. Semi-analytic studies were presented by Kounadis and Ioannidis [15,16] for the analysis of mono-symmetric beams subjected to uniform bending and axial loads. Based on Galerkin's method, Mohri et al. [17] studied the flexural–torsional and lateral postbuckling behavior of mono- and bi-symmetric simply supported beams, considering different load conditions. Pi and Bradford [18] used an accurate rotation matrix in the formulation of a finite element model for the buckling and postbuckling analysis of thin-walled straight beams. Then, Pi et al. [19–21] extended their model to analyze the flexural–torsional stability response of arches with open thin-walled section under different radial loads. They study the effects of elastic continuous restraints in [19] and the effects of the prebuckling in-plane deformations on the elastic flexural–torsional buckling in [20]. They investigated in [21] the flexural–torsional buckling and postbuckling behavior of shallow arches.

The development of beam theories usually involves some reduction of the 3-D constitutive relationship. Often this is accomplished by neglecting the stresses and strains in the transverse directions. None of the papers previously cited have considered the effect of shear flexibility. M.-Y. Kim et al. [22,23] and S.-B. Kim et al. [24] analyzed the postbuckling behavior of thin-walled frames and the buckling behavior of thin-walled tapered beams, taking into account shear deformation effects due to shear forces and warping-torsion. However, the shear deformable displacement field is introduced based on the semitangential rotations, including second-order terms of finite rotations. Machado and Cortínez [25,26] considered the effect of shear deformation to investigate the stability of composite beam. The postbuckling response of simply supported beams is analyzed in [26], where the displacements are approximated by means of trigonometric functions. In these last two references the authors showed the influence of shear deformation for different stacking sequences.

A significant amount of research has been conduced in recent years toward the development of non-linear theories of 3-D beams. However, many of this theories differ in the order of non-linearity considered in their formulation. For example, second-order displacement field has been used in a formulation of finite element models for 3-D non-linear analysis of beam structures [9,22–24,27]. This approximation has several advantages because it simplifies the coupling between the displacement and rotations, and so the tangent stiffness matrix (use for the non-linear incremental-iterative analysis) can be simplified. Therefore, this tangent matrix can be decomposed into linear and second-order (non-linear) stiffness matrices. In spite of these advantages, approximations or simplifications that are made in the earlier stages of the derivation may produce the loss of some significant terms in the non-linear strains and in the tangent stiffness matrix. Thus some inaccurate approximations in the coupling between displacement, rotations and their derivates are obtained. The loss of these terms may lead to "self-straining" caused by superimposed rigid-body motions [18,28].

The main objectives of this paper are to show the accuracy and efficiency of the proposed formulation and to investigate the effect of non-linear approximations on the buckling and postbuckling behavior of isotropic thin-walled beams subjected to different boundary conditions. Therefore, the important points presented in this work are summarized as follows:

1. The general theory of shear deformable thin-walled composite beam developed by Machado et al. [26] is used for the buckling, prebuckling and postbuckling analyses of bi-symmetric open cross-sections.
2. Ritz variational method is used for reducing the governing equation in terms of generalized coordinates to analyze the behavior of simply supported, cantilever and fixed-end beams under different load conditions. The displacements are approximated by means of a set of beam characteristic orthogonal polynomials, which satisfy the geometrical boundary conditions.
3. Buckling loads are determined from the singularity condition of the tangential stiffness matrix determinant of the structure. An incremental-iterative method based on the Newton–Raphson method combined with constant arc length is employed for the solution of non-linear equilibrium equation.

4. In addition, a practical formula is obtained to determine the critical loads of axial and lateral buckling of bi-symmetric cross-section, including prebuckling effects in the case of lateral buckling.
5. The postbuckling curves obtained with the present beam model are compared with those obtained by a shell finite element model (ABAQUS).
6. Finally, the effect of non-linear approximations is analyzed comparing the present higher-order non-linear theory with a second-order model, considering in both cases shear deformation.

2. Kinematics

A straight thin-walled beam with an arbitrary cross-section is considered (Fig. 1). The points of the structural member are referred to a Cartesian coordinate system $(x, \bar{y}, \bar{z})$, where the x-axis is parallel to the longitudinal axis of the beam while $\bar{y}$ and $\bar{z}$ are the principal axes of the cross-section. The axes y and z are parallel to the principal ones but having their origin at the shear center (SC), defined according to Vlasov's theory of isotropic beams. Midway through the thickness of each cross-sectional element is the middle surface. A plane perpendicular to the x-axis intersects the middle surface at a curve called the contour. The coordinates corresponding to points lying on the middle line are denoted as Y and Z (or $\bar{Y}$ and $\bar{Z}$). A contour (n, s, x) coordinate system is defined with s following the contour, and n perpendicular to s. This coordinate is introduced on the middle contour of the cross-section system as illustrated in Fig. 2.

$$\bar{y}(s,n) = \bar{Y}(s) - n\frac{\mathrm{d}Z}{\mathrm{d}s}, \quad \bar{z}(s,n) = \bar{Z}(s) + n\frac{\mathrm{d}Y}{\mathrm{d}s}, \tag{1}$$

$$y(s,n) = Y(s) - n\frac{\mathrm{d}Z}{\mathrm{d}s}, \quad z(s,n) = Z(s) + n\frac{\mathrm{d}Y}{\mathrm{d}s}. \tag{2}$$

On the other hand, y_0 and z_0 are the centroidal coordinates measured with respect to the SC.

$$\begin{aligned} \bar{y}(s,n) &= y(s,n) - y_0, \\ \bar{z}(s,n) &= z(s,n) - z_0. \end{aligned} \tag{3}$$

The present structural model is based on the following assumptions:

(1) The cross-section contour is rigid in its own plane.
(2) The warping distribution is assumed to be given by the Saint–Venant function for isotropic beams.
(3) Flexural rotations (about the $\bar{y}$- and $\bar{z}$-axes) are assumed to be moderate, while the twist ϕ of the cross-section can be arbitrarily large.

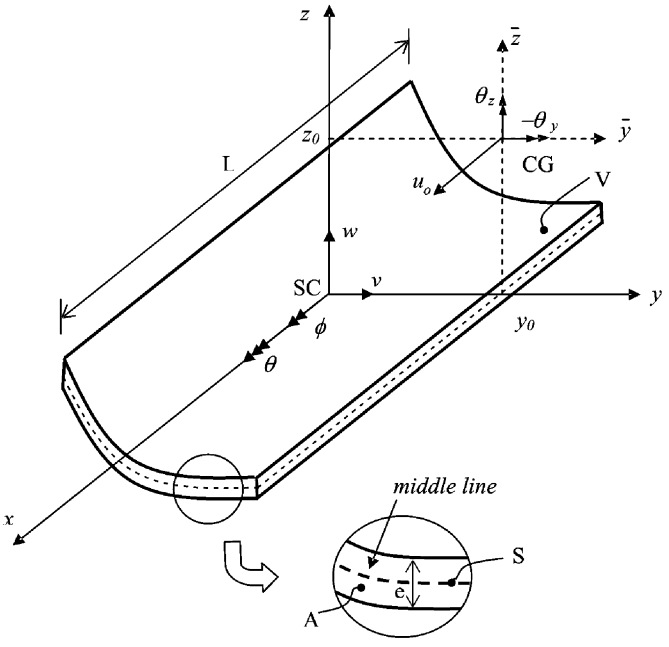

Fig. 1. General thin-walled section beam and notation for displacement measures.

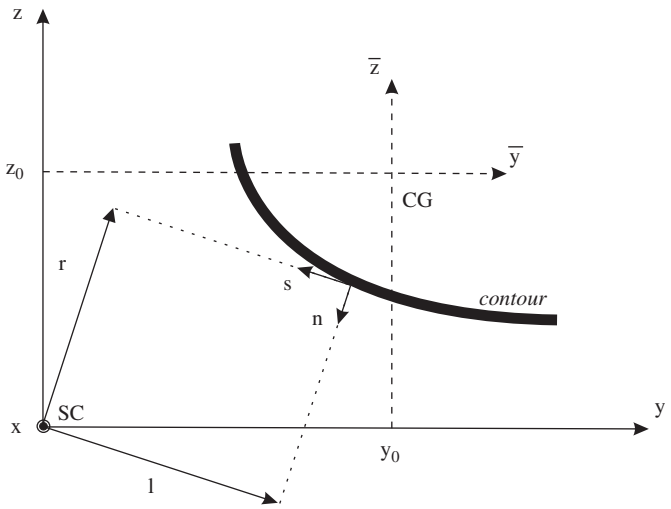

Fig. 2. Coordinate system of the cross-section.

(4) Shell force and moment resultant corresponding to the circumferential stress σ_{ss} and the force resultant corresponding to γ_{ns} are neglected.
(5) The radius of curvature at any point of the shell is neglected.
(6) Twisting linear curvature of the shell is expressed according to the classical plate theory.

2.1. Development of the displacement field

According to the hypotheses of the present structural model, the proposed displacement field Eq. (4) is based on the principle of semitangential rotation defined by Argyris [29] to avoid the difficulty due to the non-commutative nature of rotations. In this displacement field, the torsional twist terms ϕ are expressed as trigonometric functions according to hypotheses (3). The displacement field is represented by means of seven degree of freedom corresponding to three displacements (u, v and w), three measures of the rotations (ϕ, θ_y and θ_z) about the SC axis, $\bar{y}$- and $\bar{z}$-axes, respectively, and a warping variable (θ) of the cross-section. The displacement field is expressed as the following form:

$$u_x = u_o - \bar{y}(\theta_z \cos\phi + \theta_y \sin\phi) - \bar{z}(\theta_y \cos\phi - \theta_z \sin\phi) + \omega[\theta - \tfrac{1}{2}(\theta_y'\theta_z - \theta_y\theta_z')] + (\theta_z z_0 - \theta_y y_0)\sin\phi,$$
$$u_y = v - z\sin\phi - y(1-\cos\phi) - \tfrac{1}{2}(\theta_z^2\bar{y} + \theta_z\theta_y\bar{z}), \quad u_z = w + y\sin\phi - z(1-\cos\phi) - \tfrac{1}{2}(\theta_y^2\bar{z} + \theta_z\theta_y\bar{y}), \tag{4}$$

where the prime indicates differentiation with respect to x.

This expression is a generalization of others previously proposed in the literature. On the other hand, neglecting the shear flexibility ($\theta_z = v'$, $\theta_y = w'$ and $\theta = \phi'$), approximating $\cos\phi$ and $\sin\phi$ by $(1-\phi^2/2)$ and ϕ, respectively, and conserving non-linear terms up to second order, the present displacement field coincides with that developed by Fraternali and Feo [27], who formulated a moderate rotation theory of thin-walled composite beams generalizing the infinitesimal theory of sectorial areas by Vlasov [1]. Moreover, the displacement field of the classical Vlasov's [1] theory is obtained when second-order effects are ignored. As a final comparison, taking $\cos\phi = 1$ and $\sin\phi = \phi$ and disregarding the non-linear terms, the displacement field (4) coincides with the one formulated by Cortínez and Piovan [30] for linear dynamics of shear deformable thin-walled beams.

2.2. Warping displacements

In general, the contour of the cross-section will warp out of its plane as twisting occurs. The warping function ω of the thin-walled cross-section may be defined as

$$\omega(s,n) = \omega_p(s) + \omega_s(s,n), \tag{5}$$

where, ω_p and ω_s are the contour warping function and the thickness warping function, respectively. They are defined in the form [30]:

$$\omega_p(s) = \frac{1}{m}\left[\int_0^m \left(\int_{s_0}^s [r(s) - \psi(s)]\,\mathrm{d}s\right)\mathrm{d}s\right] - \int_{s_0}^s [r(s) - \psi(s)]\,\mathrm{d}s,$$
$$\omega_s(s,n) = -n\,l(s), \tag{6}$$

where m is the length of the cross-sectional thin wall and Ψ is the shear strain at the middle line, obtained by means of the Saint–Venant theory of pure torsion for isotropic beams, and normalized with respect to $\mathrm{d}\phi/\mathrm{d}x$ [31]. Besides, $r(s)$ represents the perpendicular distance from the SC to the tangent at any point of the mid-surface contour, and $l(s)$ represents the perpendicular distance from the SC to the normal at any point of the mid-surface contour, as shown in Fig. 2.

$$r(s) = -Z(s)\,\frac{\mathrm{d}Y}{\mathrm{d}s} + Y(s)\,\frac{\mathrm{d}Z}{\mathrm{d}s}, \tag{7}$$

$$l(s) = Y(s)\,\frac{\mathrm{d}Y}{\mathrm{d}s} + Z(s)\,\frac{\mathrm{d}Z}{\mathrm{d}s}. \tag{8}$$

3. The strain field

The displacements with respect to the curvilinear system (x, s, n) are obtained by means of the following expressions:

$$\bar{U} = u_x(x, s, n), \tag{9}$$

$$\bar{V} = u_y(x, s, n)\,\frac{\mathrm{d}Y}{\mathrm{d}s} + u_z(x, s, n)\,\frac{\mathrm{d}Z}{\mathrm{d}s}, \tag{10}$$

$$\bar{W} = -u_y(x, s, n)\,\frac{\mathrm{d}Z}{\mathrm{d}s} + u_z(x, s, n)\,\frac{\mathrm{d}Y}{\mathrm{d}s}. \tag{11}$$

The three non-zero components ε_{xx}, ε_{xs}, ε_{xn} of the Green's strain tensor are given by

$$\varepsilon_{xx} = \frac{\partial\bar{U}}{\partial x} + \frac{1}{2}\left[\left(\frac{\partial\bar{U}}{\partial x}\right)^2 + \left(\frac{\partial\bar{V}}{\partial x}\right)^2 + \left(\frac{\partial\bar{W}}{\partial x}\right)^2\right], \tag{12}$$

$$\varepsilon_{xs} = \frac{1}{2}\left[\frac{\partial\bar{U}}{\partial s} + \frac{\partial\bar{V}}{\partial x} + \frac{\partial\bar{U}}{\partial x}\frac{\partial\bar{U}}{\partial s} + \frac{\partial\bar{V}}{\partial x}\frac{\partial\bar{V}}{\partial s} + \frac{\partial\bar{W}}{\partial x}\frac{\partial\bar{W}}{\partial s}\right], \tag{13}$$

$$\varepsilon_{xn} = \frac{1}{2}\left[\frac{\partial\bar{U}}{\partial n} + \frac{\partial\bar{W}}{\partial x} + \frac{\partial\bar{U}}{\partial x}\frac{\partial\bar{U}}{\partial n} + \frac{\partial\bar{V}}{\partial x}\frac{\partial\bar{V}}{\partial n} + \frac{\partial\bar{W}}{\partial x}\frac{\partial\bar{W}}{\partial n}\right]. \tag{14}$$

Substituting expressions (4) into (9)–(11) and then into (12)–(14), employing the relations (1)–(3) and (5)–(8), after simplifying some higher-order terms, the components of the strain tensor are expressed in the following form:

$$\begin{aligned}
&\varepsilon_{xx} = \varepsilon_{xx}^{(0)} + n\kappa_{xx}^{(1)},\\
&\gamma_{xs} = 2\varepsilon_{xs} = \gamma_{xs}^{(0)} + n\kappa_{xs}^{(1)},\\
&\gamma_{xn} = 2\varepsilon_{xn} = \gamma_{xn}^{(0)},
\end{aligned} \tag{15}$$

where

$$\begin{aligned}
\varepsilon_{xx}^{(0)} = {} & u_o' + \tfrac{1}{2}(u_o'^2 + v'^2 + w'^2) + \omega_p[\theta' - \tfrac{1}{2}(\theta_z\theta_y'' - \theta_y\theta_z'')] + \bar{Z}[(-\theta_y' - u_o'\theta_y')\cos\phi + (\theta_z' + u_o'\theta_z')\,\mathrm{sen}\,\phi]\\
& + \bar{Y}[(-\theta_z' - u_o'\theta_z')\cos\phi - (\theta_y' + u_o'\theta_y')\,\mathrm{sen}\,\phi] + \tfrac{1}{2}\phi'^2(Y^2 + Z^2) + \tfrac{1}{2}\theta_y'^2\bar{Z}^2 + \tfrac{1}{2}\theta_z'^2\bar{Y}^2 + \theta_z'\theta_y'\bar{Z}\bar{Y}\\
& + (z_0\theta_z' - y_0\theta_y')\,\mathrm{sen}\,\phi,
\end{aligned} \tag{16}$$

$$\begin{aligned}
\kappa_{xx}^{(1)} = {} & -\frac{\mathrm{d}Z}{\mathrm{d}s}[-(\theta_z' + u_0'\theta_z')\cos\phi - (\theta_y' + u_0'\theta_y')\,\mathrm{sen}\,\phi] + \frac{\mathrm{d}Y}{\mathrm{d}s}[(-\theta_y' - u_0'\theta_y')\cos\phi + (\theta_z' + u_0'\theta_z')\,\mathrm{sen}\,\phi]\\
& - l\left[\theta' - \frac{1}{2}(\theta_z\theta_y'' - \theta_y\theta_z'')\right] - r\phi'^2 - \bar{Y}\,\frac{\mathrm{d}Z}{\mathrm{d}s}\theta_z'^2 + \bar{Z}\,\frac{\mathrm{d}Y}{\mathrm{d}s}\theta_y'^2 + \left(\bar{Y}\,\frac{\mathrm{d}Y}{\mathrm{d}s} - \bar{Z}\,\frac{\mathrm{d}Z}{\mathrm{d}s}\right)\theta_y'\theta_z',
\end{aligned} \tag{17}$$

$$\begin{aligned}
\gamma_{xs}^{(0)} = {} & \frac{\mathrm{d}Y}{\mathrm{d}s}\left[(v' - \theta_z - u_0'\theta_z)\cos\phi - z_0\frac{1}{2}(\theta_z\theta_y' - \theta_y\theta_z') + (w' - \theta_y - u_0'\theta_y)\sin\phi\right] + (r - \psi)(\phi' - \theta)\\
& + \frac{\mathrm{d}Z}{\mathrm{d}s}\left[(w' - \theta_y - u_0'\theta_y)\cos\phi + y_0\frac{1}{2}(\theta_z\theta_y' - \theta_y\theta_z') - (v' - \theta_z - u_0'\theta_z)\sin\phi\right] + \psi\left[\phi' - \frac{1}{2}(\theta_z\theta_y' - \theta_y\theta_z')\right],
\end{aligned} \tag{18}$$

$$\kappa_{xs}^{(1)} = -2\left[\phi' - \tfrac{1}{2}(\theta_z\theta_y' - \theta_y\theta_z')\right], \tag{19}$$

$$\gamma_{xn}^{(0)} = \frac{\mathrm{d}Y}{\mathrm{d}s}\left[(w' - \theta_y - u_0'\theta_y)\cos\phi + y_0\frac{1}{2}(\theta_z\theta_y' - \theta_y\theta_z') - (v' - \theta_z - u_0'\theta_z)\sin\phi\right]$$
$$- \frac{\mathrm{d}Z}{\mathrm{d}s}\left[(v' - \theta_z - u_0'\theta_z)\cos\phi - z_0\frac{1}{2}(\theta_z\theta_y' - \theta_y\theta_z') + (w' - \theta_y - u_0'\theta_y)\sin\phi\right] + l(\phi' - \theta). \tag{20}$$

4. Equilibrium equations

Taking into account the adopted assumptions, the principle of virtual work for an isotropic shell may be expressed in the form [32]:

$$\int\int (N_{xx}\delta\varepsilon_{xx}^{(0)} + M_{xx}\delta\kappa_{xx}^{(1)} + N_{xs}\delta\gamma_{xs}^{(0)} + M_{xs}\delta\kappa_{xs}^{(1)} + N_{xn}\delta\gamma_{ns}^{(0)})\,\mathrm{d}s\,\mathrm{d}x$$
$$- \int\int (\bar{q}_x\delta\bar{u}_x + \bar{q}_y\delta\bar{u}_y + \bar{q}_z\delta\bar{u}_z)\,\mathrm{d}s\,\mathrm{d}x - \int\int (\bar{p}_x\delta u_x + \bar{p}_y\delta u_y + \bar{p}_z\delta u_z)|_{x=0}\,\mathrm{d}s\,\mathrm{d}n$$
$$- \int\int (\bar{p}_x\delta u_x + \bar{p}_y\delta u_y + \bar{p}_z\delta u_z)|_{x=L}\,\mathrm{d}s\,\mathrm{d}n - \int\int\int (\bar{f}_x\delta u_x + \bar{f}_y\delta u_y + \bar{f}_z\delta u_z)\,\mathrm{d}s\,\mathrm{d}n\,\mathrm{d}x = 0, \tag{21}$$

where N_{xx}, N_{xs}, M_{xx}, M_{xs} and N_{xn} are the shell stress resultants defined according to the following expressions:

$$N_{xx} = \int_{-e/2}^{e/2}\sigma_{xx}\,\mathrm{d}n, \quad M_{xx} = \int_{-e/2}^{e/2}(\sigma_{xx}n)\,\mathrm{d}n,$$
$$N_{xs} = \int_{-e/2}^{e/2}\sigma_{xs}\,\mathrm{d}n, \quad M_{xs} = \int_{-e/2}^{e/2}(\sigma_{xs}n)\,\mathrm{d}n, \quad N_{xn} = \int_{-e/2}^{e/2}\sigma_{xn}\,\mathrm{d}n. \tag{22}$$

The beam is subjected to wall surface tractions $\bar{q}_x, \bar{q}_y$ and $\bar{q}_z$ specified per unit area of the undeformed middle surface and acting along the x-, y- and z-directions, respectively. Similarly, $\bar{p}_x$, $\bar{p}_y$ and $\bar{p}_z$ are the end tractions per unit area of the undeformed cross-section specified at $x=0$ and L, where L is the undeformed length of the beam. Besides $\bar{f}_x$, $\bar{f}_y$ and $\bar{f}_z$ are the body forces per unit of volume. Finally, denoting $\bar{u}_x$, $\bar{u}_y$ and $\bar{u}_z$ as displacements at the middle line.

Substituting Exps. (16)–(20) into (21) and integrating with respect to s, one obtains the 1-D expression for the virtual work equation given by

$$L_K + L_P = 0, \tag{23}$$

where L_K and L_P represent the virtual work contributions due to the internal and external forces, respectively.

$$L_K = \int_0^L \Big\{\delta u_0'[N + u_0'N - M_z(\theta_z'\cos\phi + \theta_y'\,\mathrm{sen}\,\phi) - M_y(\theta_y'\cos\phi + \theta_z'\,\mathrm{sen}\,\phi) - Q_y(\theta_z\cos\phi + \theta_y\,\mathrm{sen}\,\phi)$$
$$- Q_z(\theta_y\cos\phi + \theta_z\,\mathrm{sen}\,\phi)] + \delta v'(Q_y\cos\phi - Q_z\,\mathrm{sen}\,\phi + v'N) + \delta w'(Q_z\cos\phi + Q_y\,\mathrm{sen}\,\phi + w'N)$$
$$+ \delta\theta_z\left[-Q_y(1+u_0')\cos\phi + Q_z(1+u_0')\,\mathrm{sen}\,\phi + \frac{1}{2}(Q_z y_0 - Q_y z_0)\theta_y' - \frac{1}{2}T_{\mathrm{sv}}\theta_y' - \frac{1}{2}B\theta_y''\right]$$
$$+ \delta\theta_z'\left[-M_z(1+u_0')\cos\phi + M_y(1+u_0')\,\mathrm{sen}\,\phi + Nz_0\,\mathrm{sen}\,\phi + \frac{1}{2}(Q_y z_0 - Q_z y_0)\theta_y + \frac{1}{2}T_{\mathrm{sv}}\theta_y + \theta_z'P_{zz} + \theta_y'P_{yz}\right]$$
$$+ \delta\theta_y\left[-Q_z(1+u_0')\cos\phi - Q_y(1+u_0')\,\mathrm{sen}\,\phi + \frac{1}{2}(Q_y z_0 - Q_z y_0)\theta_z' + \frac{1}{2}T_{\mathrm{sv}}\theta_z' + \frac{1}{2}B\theta_z''\right]$$
$$+ \delta\theta_y'\left[-M_y(1+u_0')\cos\phi - M_z(1+u_0')\,\mathrm{sen}\,\phi - Ny_0\,\mathrm{sen}\,\phi + \frac{1}{2}(Q_z y_0 - Q_y z_0)\theta_z - \frac{1}{2}T_{\mathrm{sv}}\theta_z + \theta_z'P_{yz} + \theta_y'P_{yy}\right]$$
$$+ \delta\phi\Big[M_y(\underline{(\theta_y' + \theta_y'u_0')\,\mathrm{sen}\,\phi} + (\theta_z' + \theta_z'u_0')\cos\phi) + M_z(\underline{(\theta_z' + \theta_z'u_0')\,\mathrm{sen}\,\phi} - (\theta_y' + \theta_y'u_0')\cos\phi)$$
$$+ Q_y(\underline{(\theta_y - w' + \theta_z u_0')\,\mathrm{sen}\,\phi} - (\theta_y - w' + \theta_y u_0')\cos\phi) + N(z_0\theta_z' - y_0\theta_y')\cos\phi$$
$$+ Q_z(\underline{(\theta_y - w' + \theta_y u_0')\,\mathrm{sen}\,\phi} + (\theta_z - v' + \theta_z u_0')\cos\phi)\Big] + \delta\theta_z''\frac{1}{2}B\theta_y - \delta\theta_y''\frac{1}{2}B\theta_z$$
$$+ \delta\phi'[T_w + T_{\mathrm{sv}} + B_1\phi'] + \delta\theta' B - \delta\theta T_w\Big\}\,\mathrm{d}x, \tag{24}$$

$$
\begin{aligned}
L_P = \int_0^L \Big\{ & -q_x\delta u_0 - q_y\delta v - q_z\delta w - b\delta\theta - \delta\theta_z'\frac{1}{2}b\theta_y + \delta\theta_y'\frac{1}{2}b\theta_z \\
& + \delta\theta_z\left[m_z\cos\phi - (m_y + z_0q_x)\sin\phi + \frac{1}{2}b\theta_y' + \frac{1}{2}\lambda_{mx}\theta_y + \lambda_y\theta_z\right] \\
& + \delta\theta_y\left[m_y\cos\phi + (m_z + y_0q_x)\sin\phi - \frac{1}{2}b\theta_z' + \frac{1}{2}\lambda_{mx}\theta_z + \lambda_z\theta_y\right] \\
& + \delta\phi[-m_x\cos\phi - (m_z\theta_z + m_y\theta_y)\sin\phi - (m_y + z_0q_x)\theta_z\cos\phi \\
& + (m_z + y_0q_x)\theta_y\cos\phi + \sin\phi(\lambda_y + \lambda_z + z_0q_z + y_0q_y)]\Big\}\,\mathrm{d}x \\
& + \Big|-\bar{N}\delta u_0 - \bar{Q}_y\delta v - \bar{Q}_z\delta w - \bar{B}\delta\theta - \delta\theta_z'\frac{1}{2}\theta_y\bar{B} + \delta\theta_y'\frac{1}{2}\theta_z\bar{B} \\
& + \delta\theta_z\left[\bar{M}_z\cos\phi - (\bar{M}_y + \bar{N}z_0)\sin\phi + \frac{1}{2}\theta_y'\bar{B} + \theta_z\bar{\lambda}_y + \frac{1}{2}\theta_y\bar{\lambda}_{mx}\right] \\
& + \delta\theta_y\left[\bar{M}_y\cos\phi + (\bar{M}_z + \bar{N}y_0)\sin\phi - \frac{1}{2}\theta_z'\bar{B} + \theta_y\bar{\lambda}_z + \frac{1}{2}\theta_z\bar{\lambda}_{mx}\right] \\
& + \delta\phi\left[-\bar{M}_x\cos\phi - \sin\phi(\bar{M}_z\theta_z + \bar{M}_y\theta_y) - \cos\phi(\bar{M}_y\theta_z - \bar{M}_z\theta_y + \bar{N}z_0\theta_z - \bar{N}y_0\theta_y) + \bar{B}_1\sin\phi\right]\Big|_{x=0}^{x=L},
\end{aligned}
\tag{25}
$$

where q_x, q_y, q_z, m_x, m_y, m_z, b, λ_y, λ_z and λ_{mx} are resultants of the applied wall surface tractions and $\bar{N}$, $\bar{Q}_y$, $\bar{Q}_z$, $\bar{M}_z$, $\bar{M}_y$, $\bar{B}$, $\bar{M}_x$, $\bar{\lambda}_y$, $\bar{\lambda}_z$, $\bar{\lambda}_{mx}$ and $\bar{B}_1$ represent the resultants of the applied end tractions.

5. Beam forces and constitutive equations

In the above expressions, the following 1-D beam forces, in terms of the shell stress resultants, have been defined as

$$
\begin{aligned}
& N = \int N_{xx}\,\mathrm{d}s, \quad M_Y = \int\left(N_{xx}\bar{Z} + M_{xx}\frac{\mathrm{d}Y}{\mathrm{d}s}\right)\mathrm{d}s, \quad M_Z = \int\left(N_{xx}\bar{Y} - M_{xx}\frac{\mathrm{d}Z}{\mathrm{d}s}\right)\mathrm{d}s, \\
& Q_Z = \int\left(N_{xs}\frac{\mathrm{d}Z}{\mathrm{d}s} + N_{xn}\frac{\mathrm{d}Y}{\mathrm{d}s}\right)\mathrm{d}s, \quad Q_Y = \int\left(N_{xs}\frac{\mathrm{d}Y}{\mathrm{d}s} - N_{xn}\frac{\mathrm{d}Z}{\mathrm{d}s}\right)\mathrm{d}s, \quad T_w = \int(N_{xs}(r-\psi) + N_{xn}l)\,\mathrm{d}s, \\
& B = \int(N_{xx}\omega_p - M_{xx}l)\,\mathrm{d}s, \quad T_{\mathrm{sv}} = \int(N_{xs}\psi - 2M_{xs})\,\mathrm{d}s,
\end{aligned}
\tag{26}
$$

where N corresponds to the axial force, Q_y and Q_z to shear forces, M_y and M_z to bending moments about $\bar{y}$- and $\bar{z}$-axis, respectively, B to the bimoment, T_w to the flexural–torsional moment and T_{sv} to the Saint–Venant torsional moment (see Fig. 3). In addition, four high-order stress resultants have been defined:

$$
\begin{aligned}
& B_1 = \int[N_{xx}(Y^2 + Z^2) - 2M_{xx}r]\,\mathrm{d}s, \quad P_{yy} = \int\left[N_{xx}\bar{Z}^2 + 2M_{xx}\bar{Z}\frac{\mathrm{d}Y}{\mathrm{d}s}\right]\mathrm{d}s, \\
& P_{zz} = \int\left[N_{xx}\bar{Y}^2 - 2M_{xx}\bar{Y}\frac{\mathrm{d}Z}{\mathrm{d}s}\right]\mathrm{d}s, \quad P_{yz} = \int\left[N_{xx}\bar{Y}\bar{Z} + M_{xx}\left(\bar{Y}\frac{\mathrm{d}Y}{\mathrm{d}s} - \bar{Z}\frac{\mathrm{d}Z}{\mathrm{d}s}\right)\right]\mathrm{d}s.
\end{aligned}
\tag{27}
$$

In Exps. (26) and (27) the integration is carried out over the entire length of the mid-line contour.

Assuming the linear elastic material, the force–displacement relations are obtained applying Hook's law. This constitutive law can be expressed in terms of a beam stiffness matrix $[K]$ as defined in Appendix. Re-arranging the virtual work (23) in terms of the beam forces and moments, the generalized strains can be identified as:

$$
\begin{aligned}
& \textit{corresponding to } N: \quad \mathrm{ED}_1 = u_o' + \frac{1}{2}(u_o'^2 + v'^2 + w'^2) + (z_0\theta_z' - y_0\theta_y')\,\mathrm{sen}\,\phi, \\
& \textit{corresponding to } M_y: \quad \mathrm{ED}_2 = (-\theta_y' - u_o'\theta_y')\cos\phi + (\theta_z' + u_o'\theta_z')\,\mathrm{sen}\,\phi, \\
& \textit{corresponding to } M_z: \quad \mathrm{ED}_3 = (-\theta_z' - u_o'\theta_z')\cos\phi - (\theta_y' + u_o'\theta_y')\,\mathrm{sen}\,\phi,
\end{aligned}
$$

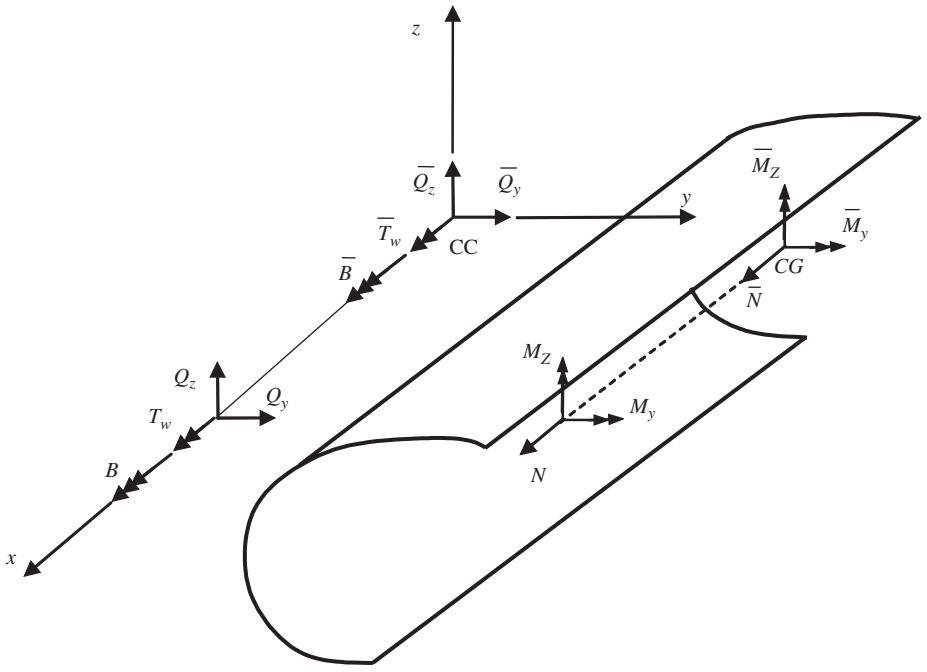

Fig. 3. Stress resultants of a thin-walled cross-section and member end forces.

$$\textit{corresponding to } B: \quad \mathrm{ED}_4 = \theta' - \frac{1}{2}(\theta_z\theta''_y - \theta_y\theta''_z),$$

$$\textit{corresponding to } Q_y: \quad \mathrm{ED}_5 = (v' - \theta_z - u'_0\theta_z)\cos\phi - z_0\frac{1}{2}(\theta_z\theta'_y - \theta_y\theta'_z) + (w' - \theta_y - u'_0\theta_y)\,\mathrm{sen}\,\phi,$$

$$\textit{corresponding to } Q_z: \quad \mathrm{ED}_6 = (w' - \theta_y - u'_0\theta_y)\cos\phi + y_0\frac{1}{2}(\theta_z\theta'_y - \theta_y\theta'_z) - (v' - \theta_z - u'_0\theta_z)\,\mathrm{sen}\,\phi,$$

$$\textit{corresponding to } T_w: \quad \mathrm{ED}_7 = \phi' - \theta,$$

$$\textit{corresponding to } T_{\mathrm{sv}}: \quad \mathrm{ED}_8 = \phi' - \frac{1}{2}(\theta_z\theta'_y - \theta_y\theta'_z),$$

$$\textit{corresponding to } B_1: \quad \mathrm{ED}_9 = \frac{\phi'^2}{2},$$

$$\textit{corresponding to } P_{yy}: \quad \mathrm{ED}_{10} = \frac{\theta'^2_y}{2},$$

$$\textit{corresponding to } P_{zz}: \quad \mathrm{ED}_{11} = \frac{\theta'^2_z}{2},$$

$$\textit{corresponding to } P_{yz}: \quad \mathrm{ED}_{12} = \theta'_y\theta'_z. \tag{28}$$

These generalized strains correspond to the axial strain (ED_1), the two bending curvatures (ED_2 and ED_3), the torsional curvature (ED_4), the two transverse shear strain (ED_5 and ED_6), the transverse shear strain due to warping (ED_7), the rate of twist and a non-linear term (ED_8 and ED_9), the higher order axial terms (ED_{10}, ED_{11} and ED_{12}).

6. The discrete equilibrium problem

In order to perform the non-linear analysis, the Ritz variational method is used for reducing the governing equation in terms of generalized coordinates. From the reduced system, the buckling loads are first determined from the singularity condition of the tangential stiffness matrix determinant. Then, an incremental-iterative method based on the Newton–Raphson method combined with constant arc length is employed for the solution of non-linear equilibrium equation. The motion equations (23) are discretized to analyze the behavior of simply supported, cantilever and fixed-end beams under different load conditions.

In the case of simply supported beams, the displacement modes are approximated by means of the following functions, which are compatible with the boundary conditions of the beam:

$$\begin{aligned} u &= u_0 \frac{x}{L}, \\ v &= v_0 \operatorname{sen}\left(\frac{\pi}{L}x\right), \quad \theta_z = \theta_{z_0} \cos\left(\frac{\pi}{L}x\right), \\ w &= w_0 \operatorname{sen}\left(\frac{\pi}{L}x\right), \quad \theta_y = \theta_{y_0} \cos\left(\frac{\pi}{L}x\right), \\ \phi &= \phi_0 \operatorname{sen}\left(\frac{\pi}{L}x\right), \quad \theta = \theta_0 \cos\left(\frac{\pi}{L}x\right), \end{aligned} \tag{29}$$

where u_0, v_0, w_0, θ_{z_0}, θ_{y_0}, ϕ_0 and θ_0 are the associated displacement amplitudes. Besides, these functions represent the exact solution to solve the linear equilibrium equations.

For the cantilever and fixed-end beams, the variational equation (23) is discretized by using beam characteristic orthogonal polynomials which satisfy the geometrical boundary conditions and are generated by using the Gram–Schmidt process.

$$U = \sum_{i=1}^{n} c_i \xi_i(x), \tag{30}$$

where U represent each of the displacements and c_i are the undetermined arbitrary coefficients. The polynomials $\xi_i(x)$ are generated as follows [33]:

$$\xi_2(x) = (x - B_2)\xi_1(x), \ldots, \xi_k(x) = (x - B_k)\xi_{k-1}(x) - C_k\xi_{k-2}(x),$$

where

$$B_k = \frac{\int_0^L x\xi_{k-1}^2(x)\,\mathrm{d}x}{\int_0^L \xi_{k-1}^2(x)\,\mathrm{d}x}, \quad C_k = \frac{\int_0^L x\xi_{k-1}(x)\xi_{k-2}(x)\,\mathrm{d}x}{\int_0^L \xi_{k-2}^2\,\mathrm{d}x}. \tag{31}$$

The first member of the orthogonal polynomial $\xi_1(x)$ is chosen as the simplest polynomial (of the least order) that satisfies the boundary conditions. In order to obtain sufficient accurate results, four terms ($n = 4$) are taken for each one of the flexural–torsional displacements. After integration along the beam length according to the adopted functions for the displacements, a coupled and strongly non-linear algebraic system is obtained. This resulting system has an extremely complicated form, for this reason, it is not presented here.

7. Analytical solutions for axial and lateral buckling

In this section, as a special case, the analytical solutions are derived for the flexural–torsional and lateral buckling of bi-symmetric cross-section.

7.1. Lateral buckling

When the beam is loaded in its plane of symmetry it initially deflects (Fig. 4a). However, at a certain level of the applied load, the beam may buckle laterally, while the cross-sections of the beam rotate simultaneously about the beam's axis (Fig. 4b). This phenomenon is called lateral buckling, and the load value at which buckling occurs is the critical load. The initial deflection corresponds to the prebuckling state, also called "the fundamental state". When the buckling load is reached, the behavior of the beam is initially flexural–torsional and corresponds to the secondary or equilibrium path.

The stability analysis of bi-symmetric thin-walled beams is analyzed by taking into account the initial deflection in the pre-buckling state (fundamental state). The displacement components in the fundamental state are in the form $\{u, v, \theta_z, w, \theta_y, \phi, \theta\}^{\mathrm{t}} = \{0, 0, 0, w, \theta_y, 0, 0\}^{\mathrm{t}}$, i.e. the beam deforms in the loading plane. It is reasonable to assume that the fundamental state may be obtained with sufficient approximation by means of the linearized theory [30]. Therefore, neglecting all the non-linear terms in (23) and applying the variational calculus, the differential equations of equilibrium are obtained. These last are easily solved in a closed form in order to determine the prebuckling displacements in the loading plane.

For the case of simply supported beams subjected to uniform bending, the prebuckling displacements are given by the following expressions:

$$w = \frac{\mathrm{Mo}}{2\mathrm{EI}_y}(Lx - x^2), \quad \theta_y = \frac{\mathrm{Mo}}{2\mathrm{EI}_y}(L - 2x). \tag{32}$$

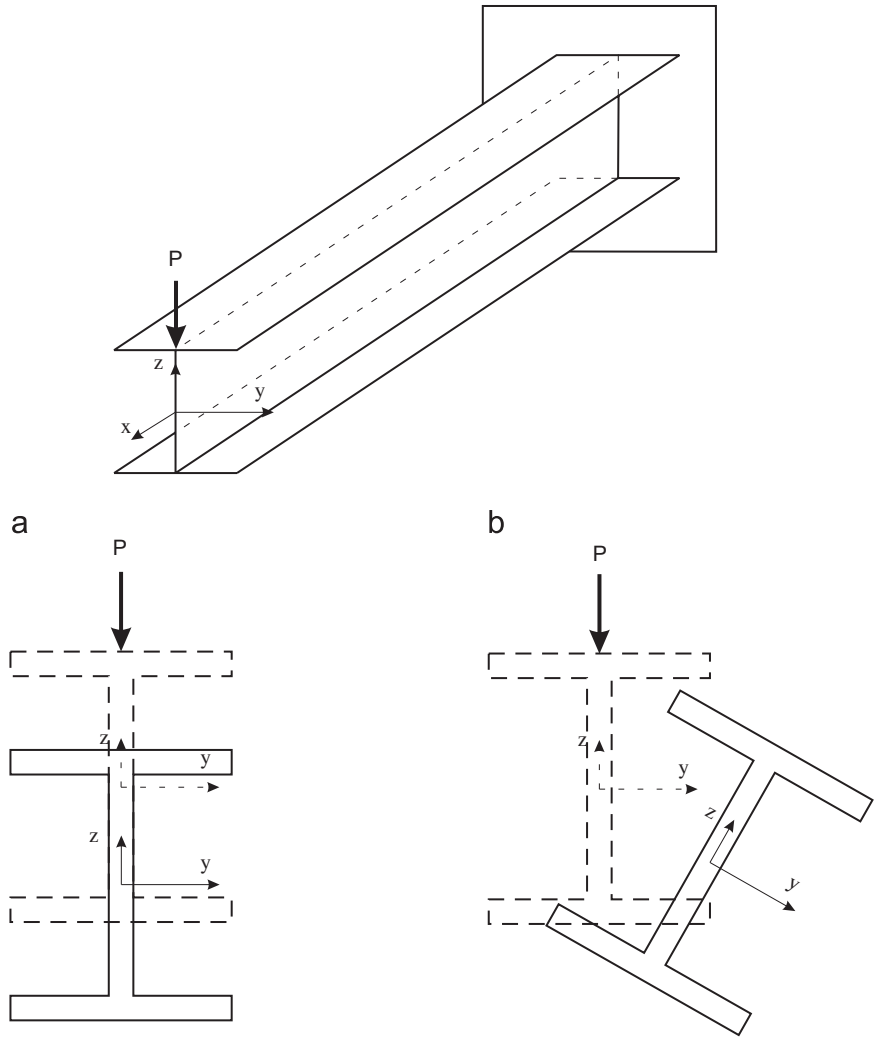

Fig. 4. Deformed shape corresponding to: (a) prebuckling state (fundamental state) and (b) postbuckling state (secondary state).

To determine the lateral buckling considering prebuckling deformation, Exp. (32) are substituted into (23), the resultant variational equation is discretized by means of the trigonometric functions defined in (29) and then the tangential stiffness matrix is obtained [34]. This procedure leads to the following expression for the tangential matrix evaluated in the fundamental state:

$$\mathbf{Kt} = \begin{bmatrix} \dfrac{GS_y\pi^2}{L^2} & -\dfrac{GS_y\pi}{L} & 0 & 0 \\ -\dfrac{GS_y\pi}{L} & GS_y + EI_z\dfrac{\pi^2}{L^2} & -Mo\left(1-\dfrac{EI_z}{EI_y}-\dfrac{GJ}{4EI_y}\right)\dfrac{\pi}{L} & \dfrac{EC_w\pi^2 Mo}{4EI_yL^2} \\ 0 & -Mo\left(1-\dfrac{EI_z}{EI_y}-\dfrac{GJ}{4EI_y}\right)\dfrac{\pi}{L} & -\dfrac{Mo^2}{EI_y}\left(1-\dfrac{EI_z}{EI_y}\right)+(GJ+GS_w)\dfrac{\pi^2}{L^2} & -\dfrac{GS_w\pi}{L} \\ 0 & \dfrac{EC_w\pi^2 Mo}{4EI_yL^2} & -\dfrac{GS_w\pi}{L} & GS_w + EC_w\dfrac{\pi^2}{L^2} \end{bmatrix}, \tag{33}$$

where $EI_y$is the flexural stiffness, GS_z and GS_y are the shear stiffnesses. The definitions of these stiffnesses are given in Appendix. The buckling state is given by the condition of singularity of this matrix [34]:

$$\det(\mathbf{Kt}) = 0. \tag{34}$$

Hence, a quadratic equation is obtained for the external load, the solution of this equation allows obtaining the critical values.

Table 1
Parameters in Eqs. (36)–(37)

Simply supported beam	C_1	C_2	β	δ
(a) End moments	1	0	0.5	0
(b) Uniformly distributed load ($M_{cr} = q_z L^2/8$)	1.141	0.459	0.033	0.214
(c) Concentrated force ($M_{cr} = PL/4$)	1.423	0.554	0.076	0.083

Following the same procedure and only changing Exp. (32) for different loads conditions (distributed load and concentrated load), it is possible to obtain a unified simple formula for the equivalent moment defined as

$$M_{cr} = \begin{cases} M_{y0} & \text{for uniform bending,} \\ q_z L^2/8 & \text{for a uniformly distributed load per unit length } q_z, \\ PL/4 & \text{for a concentrated force } P \text{ at the middle of the span.} \end{cases} \tag{35}$$

The explained technique leads to the following unified expression of the critical moment for the three loading cases analyzed:

$$M_{cr} = C_1 \alpha \mathrm{EI}_z \frac{\pi^2}{L^2} \left[-C_2 e_z \alpha + \sqrt{\frac{\mathrm{GS}_w \mathrm{GJ} + \mathrm{EC}_w(\mathrm{GS}_w + \mathrm{GJ})\dfrac{\pi^2}{L^2}}{\mathrm{EI}_z \dfrac{\pi^2}{L^2}\left(\mathrm{GS}_w + \mathrm{EC}_w \dfrac{\pi^2}{L^2}\right)} + (C_2 e_z \alpha)^2} \right], \tag{36}$$

$$\alpha = \frac{1}{\sqrt{\left(1 - \dfrac{\mathrm{EI}_z}{\mathrm{EI}_y}\right)\left(1 - \beta\dfrac{\mathrm{GJ}}{\mathrm{EI}_y} - \beta\dfrac{\mathrm{EC}_w \mathrm{GS}_w \pi^2}{\mathrm{EI}_y(\mathrm{GS}_w L^2 + \mathrm{EC}_w \pi^2)}\right) - \delta\dfrac{\mathrm{EI}_z}{\mathrm{GS}_y}\dfrac{\pi^2}{L^2}\left[1 - \dfrac{\mathrm{GS}_y}{\mathrm{GS}_z}\left(0.71 - \dfrac{\mathrm{GS}_y}{\mathrm{GS}_z}0.29\right)\right]}}, \tag{37}$$

where C_1, C_2, β and δ are approximate constants presented in Table 1.

Exp. (36) also gives the corresponding equivalent moments according to the linearized theory, which does not account for the prebuckling deflection, if one takes $\alpha = 1$. These constants are exact, from the point of view of the linear theory, for uniform bending and approximate for the other loading cases.

Therefore, the presence of the α coefficient reveals the dependence of the prebuckling effect with respect to the relation between the bending stiffnesses EI_z and EI_y in the case of uniform bending. For the other two load conditions, α also depends on the bending and shear stiffnesses ($\delta \neq 0$).

As a particular case, neglecting shear deformation, the Exp. (36) takes the following form for uniform bending:

$$M_{cr} = \frac{\dfrac{\pi}{L}\sqrt{\mathrm{EI}_z\left(\mathrm{GJ} + \mathrm{EC}_w\dfrac{\pi^2}{L^2}\right)}}{\sqrt{\left(1 - \dfrac{\mathrm{EI}_z}{\mathrm{EI}_y}\right)\left(1 - \dfrac{\mathrm{GJ}}{2\mathrm{EI}_y} - \dfrac{\mathrm{EC}_w}{2\mathrm{EI}_y}\dfrac{\pi^2}{L^2}\right)}}. \tag{38}$$

This last expression coincides with the closed-form solution obtained by Pi and Trahair [35] for elastic lateral buckling, considering prebuckling deflections.

7.2. Flexural–torsional buckling

A general analytical model applicable to the flexural and torsional buckling of a simply supported thin-walled beam subjected to axial load is developed. In the case of bi-symmetrical beam, there are three buckling modes corresponding either to bending or torsion (see Fig. 5). Applying the same procedure as explained above, the expression for the tangential matrix

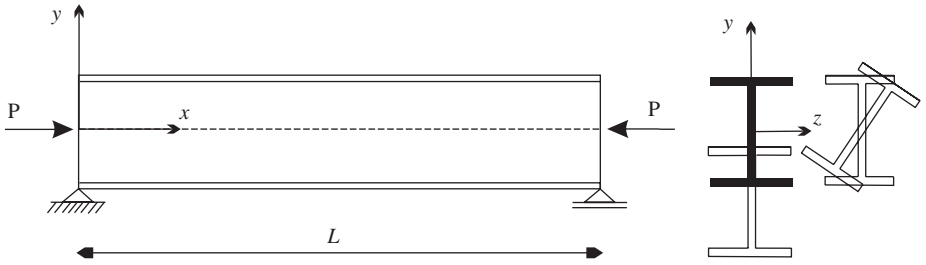

Fig. 5. Simply supported beam subjected to axial load and buckling shape modes.

yields

$$\mathbf{Kt}=\begin{bmatrix} \dfrac{(\mathrm{GS}_y+P)\pi^2}{L^2} & -\dfrac{\mathrm{GS}_y\pi}{L} & 0 & 0 & 0 & 0 \\ & \mathrm{GS}_y+\dfrac{\mathrm{EI}_z\pi^2}{L^2} & 0 & 0 & 0 & 0 \\ & & \dfrac{(\mathrm{GS}_z+P)\pi^2}{L^2} & -\dfrac{\mathrm{GS}_z\pi}{L} & 0 & 0 \\ & & & \mathrm{GS}_z+\dfrac{\mathrm{EI}_y\pi^2}{L^2} & 0 & 0 \\ & \text{Sym} & & & \dfrac{\pi^2(\mathrm{GJ}+I_0P+\mathrm{GS}_w)}{L^2} & -\dfrac{\mathrm{GS}_w\pi}{L} \\ & & & & & \mathrm{GS}_w+\dfrac{\mathrm{EC}_w\pi^2}{L^2} \end{bmatrix}. \tag{39}$$

Therefore, the condition of singularity of this matrix leads to the following three expressions of critical load:

$$Pz=\frac{\mathrm{EI}_z\mathrm{GS}_y\pi^2}{\mathrm{GS}_yL^2+\mathrm{EI}_z\pi^2}, \tag{40}$$

$$Py=\frac{\mathrm{EI}_y\mathrm{GS}_z\pi^2}{\mathrm{GS}_zL^2+\mathrm{EI}_y\pi^2}, \tag{41}$$

$$P\phi=\frac{L^2\mathrm{GS}_w\mathrm{GJ}+\mathrm{EC}_w\pi^2(\mathrm{GJ}+\mathrm{GS}_w)}{I_0(\mathrm{GS}_wL^2+\mathrm{EC}_w\pi^2)}, \tag{42}$$

where I_0 is the inertia polar moment about the SC. In these expressions, Py, Pz and $P\phi$ are the buckling loads of a simply supported beam, corresponding to bending and torsion mode.

8. Applications and numerical results

The purpose of this section is to apply the present method in order to illustrate the accuracy and practical usefulness of this formulation; numerical solutions for flexural, lateral–torsional buckling and postbuckling of thin-walled beams are presented and discussed.

8.1. Simply supported beam subjected to distributed load

In this example a simply supported I-beam under distributed load is considered, for three load positions, as shown in Fig. 6. The geometrical and material properties are $L=6\,\mathrm{m}$, $h=0.6\,\mathrm{m}$, $b=0.6\,\mathrm{m}$, $e=0.03\,\mathrm{m}$, $E=200\,\mathrm{GPa}$ and $\mu=0.3$.

The present theory is applied considering both linear and geometrically non-linear buckling behavior. Besides, in the load critical tables the following notation is used:

LB: denotes buckling values determined by the linear or classical theory, disregarding non-linear effects and without considering prebuckling deformations.

NLB: denotes values obtained by means of the present complete non-linear model, accounting for prebuckling deflections.

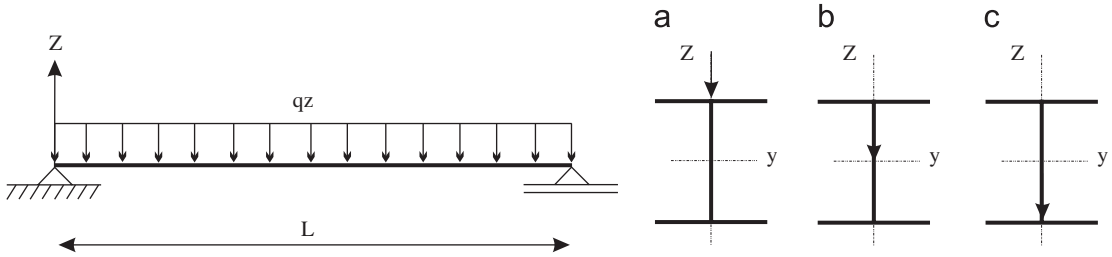

Fig. 6. Simply supported beam subjected to distributed load applied in different heights.

Table 2
Buckling load of simply supported I-beam ($q_z \times 10^6$ Nm)

Load height	Analysis	Beam model (numeric)	Analytical Exp. (36)
Top	NLB	3.81	3.85
	LB	3.45	3.45
Shear center	NLB	6.13	6.20
	LB	5.17	5.17
Bottom	NLB	9.88	10.00
	LB	7.76	7.76

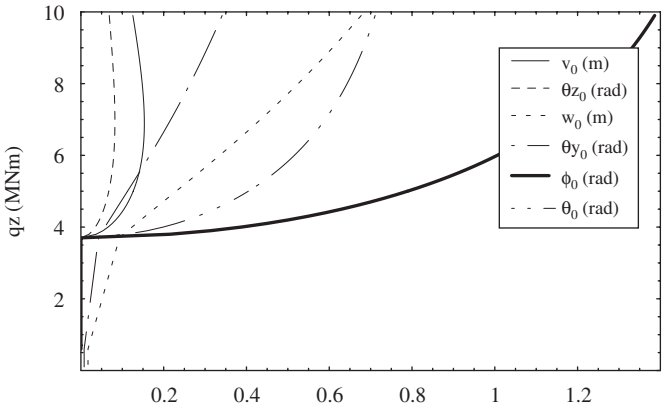

Fig. 7. Postbuckling paths of a simply supported beam, load on top flange.

In particular, the former theory (LB) was modeled by discarding effects due to large rotations up to the critical equilibrium state. The buckling loads for three different load heights are shown in Table 2, comparing the analytical (Exp. 36) and numerical results obtained from the non-linear analysis.

It is important to mention that the numerical buckling loads correspond to the bifurcation points observed in the postbuckling response, see Figs. 7–9, for the load applied on the top flange, SC and bottom flange, respectively. It can be seen that the predictions by the non-linear algorithm are in good agreement with those obtained with the closed-form solution, Exp. (36).

The buckling loads computed from the linear stability (LB) analysis show a very conservative behavior compared with those computed from the non-linear stability (NLB). The effect of accounting for in-plane prebuckling deformations in the determination of critical loads is quite significant when the load is applied at the bottom flange. In this last case, the beam behavior is stiffer in the prebuckling state and the vertical displacement increases considerably. This value can reach about $w = 0.25$ m in comparison with the value of about $w = 0.1$ m when the load is applied on the top flange. This can explain the great difference (about 20%) between the buckling loads computed with the classical theory with the results obtained with the non-linear model. So the geometrically non-linear effects increase when the vertical displacement, corresponding to the prebuckling state, increases too.

In the same way as the lateral buckling strength depends on the load height parameter, the margins of postbuckling strength are smaller when the load is applied on the top flange.

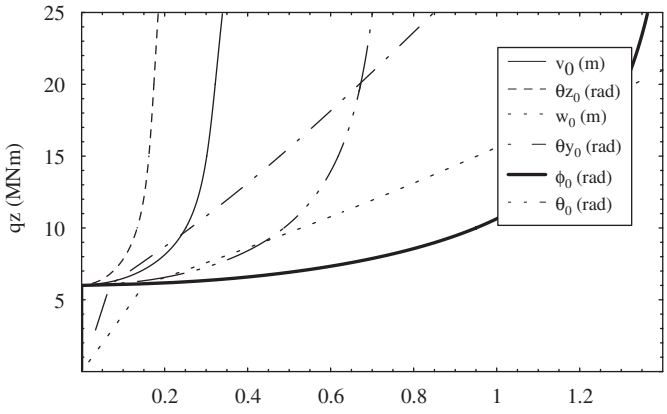

Fig. 8. Postbuckling paths of a simply supported beam, load on shear center.

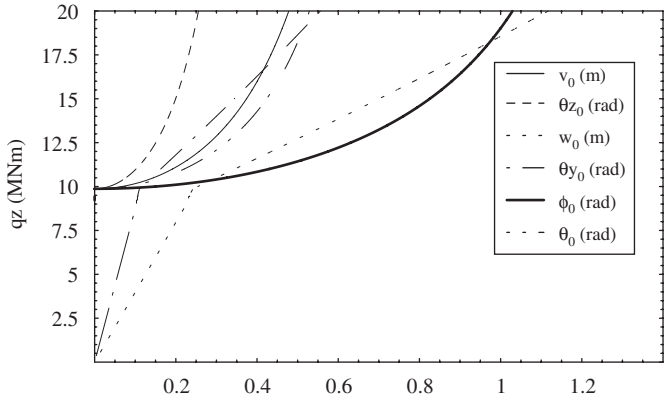

Fig. 9. Postbuckling paths of a simply supported beam, load on bottom flange.

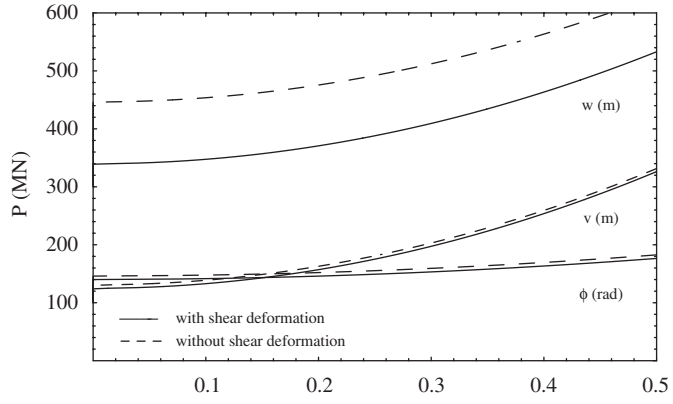

Fig. 10. Flexural–torsional postbuckling paths of a simply supported beam, $L = 4\,\mathrm{m}$.

8.2. *Bi-symmetric open section subjected to an axial force*

The example considered is a simply supported bi-symmetric-I section whose geometrical and material properties are the same as the previous example. In this example ($y_0 = z_0 = 0$), the equilibrium equations are non-linear but uncoupled. Therefore, there are three buckling modes corresponding either to bending or torsion. The flexural mode corresponding to displacement v (y-direction) has the smallest buckling load, as is illustrated in Fig. 10, where the postbuckling paths are presented for the three buckling modes. Moreover, two models are compared: the present theory (considering shear deformation) and results obtained by neglecting shear flexibility. The figure shows that the postbuckling equilibrium paths are stable and symmetric. Shear effect reduces the values of

Table 3
Buckling load of simply supported I-beam ($P_{cr} \times 10^6$ N)

h/L	Shear deformation	Buckling mode (Exp. (40)–(42))		
		Bending-v	Torsional-ϕ	Bending-w
0.10	With	58.05	71.89	180.38
	Without	59.29	73.13	207.41
0.15	With	127.27	141.12	340.70
	Without	133.41	147.25	447.66
0.20	With	218.45	232.30	518.78
	Without	237.16	251.01	829.64

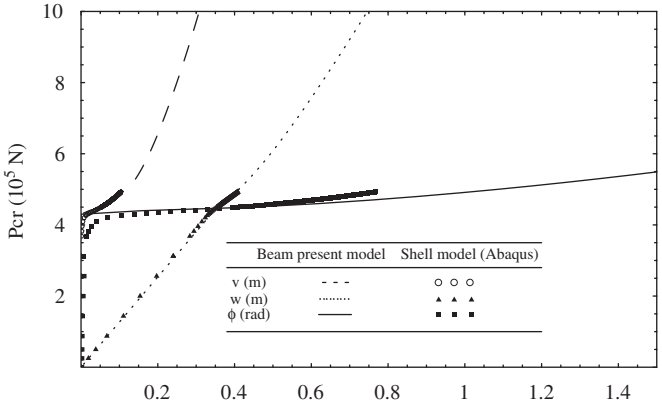

Fig. 11. Postbuckling paths of a cantilever beam, load on top flange.

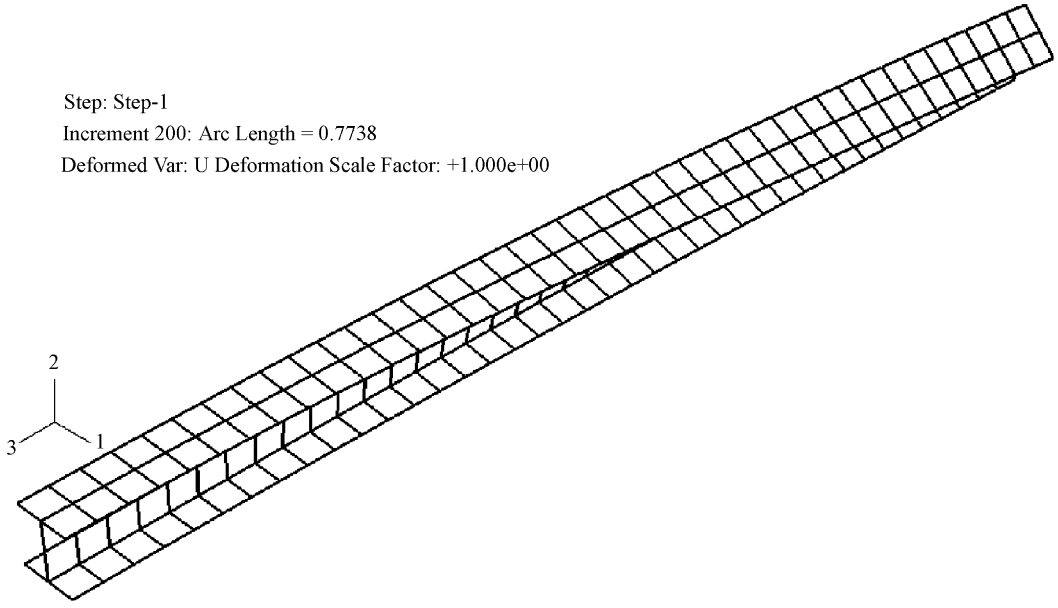

Fig. 12. Deformed shape corresponding to the postbuckling state for a cantilever beam.

the equilibrium path with respect to the non-shearable theory and this effect is considerably more important for the vertical bending mode.

In Table 3, the buckling loads are given for both models (with and without shear deformation) and considering three different beam lengths. It is observed that the influence of shear deformation is more significant on the buckling behavior as the beam length decreases. This difference can reach about 60% for the vertical buckling mode and for a beam of $L = 3$ m.

Table 4
Buckling load of cantilever I-beam ($P_{cr} \times 10^5$ N)

Load height	Analysis	Beam model (present)	Shell model (Abaqus)
Top	NLB	4.37	4.32
	LB	4.27	4.19
Shear center	NLB	9.45	9.50
	LB	8.84	8.52
Bottom	NLB	14.30	14.29
	LB	12.02	11.83

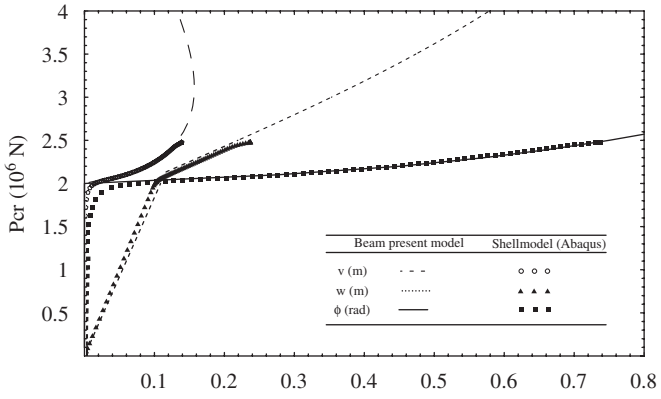

Fig. 13. Postbuckling paths of a simply supported beam loaded on top flange.

8.3. Cantilever beam subjected to end force

The example considered is a cantilever beam subjected to end force applied in three different positions of the free end. The geometrical and material properties are the same as the previous example. The accuracy of the proposed formulation is checked by comparing results (i.e. buckling loads and postbuckling response) with those solutions obtained by Abaqus's shell element. The beam is idealized by 240 four-node shell elements (S4). First, an eigenvalue buckling analysis is performed on the "perfect" structure using LANCZOS solver to establish probable collapse modes and to verify that the mesh discretizes those modes accurately. In the second analysis an imperfection is introduced in the geometry by addition of the buckling modes to the "perfect" geometry using the IMPERFECTION option. A geometrically non-linear load–displacement analysis of the structure containing the imperfections is performed using the Riks method. In this way, the Riks method can be used to perform postbuckling analyses. The magnitudes of the perturbations are typically a small percent of a relative structural dimension and in this case the associated scale factor used is 0.005.

The lateral postbuckling curves are shown in Fig. 11, for a beam length $L = 12$ m and for load applied on the top flange. The beam behavior is represented by the vertical displacement w (corresponding to the load in-plane movement), torsional twist ϕ and lateral displacement v. The postbuckling equilibrium paths are stable and symmetric. The load-deflection curve (v) has a stiffer behavior in the postbuckling state in comparison with the other displacements. The initial postbuckling paths obtained with the present beam are in good agreement with those obtained with shell finite element model. The deformed state of the thin-walled beam obtained with Abaqus is shown in Fig. 12, the step correspond to the twisting amplitude of 0.8 rad. On the other hand, the bifurcation values agree with the buckling load presented in Table 4.

The buckling loads of the present study are compared with the results obtained from the linear analysis, for three load height cases. The influence of the geometrically non-linear effects (prebuckling) on the buckling loads is notable, and it becomes greater when the load is applied to the bottom flange, as in the first example (8.1). For this load condition the discrepancy can reach about 16%.

8.4. Simply supported I-beam subjected to a concentrated force

A fixed-end beam loaded by a transverse force at the middle of the span is considered. The geometrical and material properties are the same as the previous example. The load–displacement curves are shown in Fig. 13, for a load applied on the top flange. The postbuckling equilibrium paths are similar to the previous case, but for this boundary condition the beam response shows a

Table 5
Buckling load of fixed-end beam ($P_{cr} \times 10^6$ N)

Load height	Analysis	Beam model (numeric)	Analytical Exp. (36)	Shell model (Abaqus)
Top	NLB	2.00	2.08	2.00
	LB	1.86	1.86	1.86

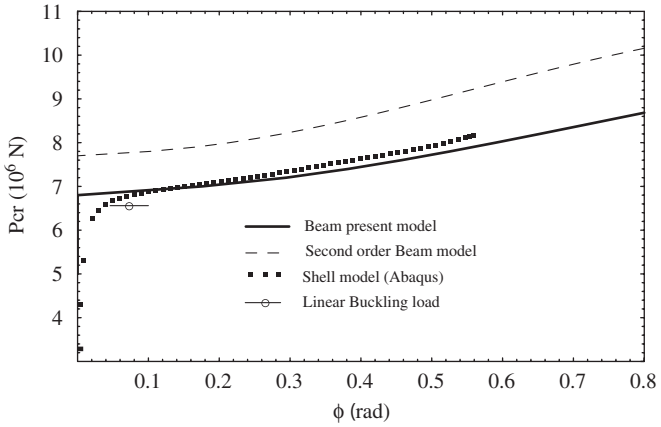

Fig. 14. Comparison of non-linear models in the postbuckling behavior, load on top flange.

stiffer behavior, as much in the critical condition as in the prebuckling state. Besides, comparing the postbuckling twisting curves the load-carrying capacity is larger in the case of simply supported beam.

On the other hand, the bifurcation values agree with the buckling load presented in Table 5. In this case, the effect of the geometrically non-linear effects is about 7% and is a little greater than in the previous example (about 3%).

8.5. Comparison of the present model against a moderate rotation theory

The purpose of this example is to show the effect of the degree of non-linearity adopted in the displacement field (4) on the lateral postbuckling behavior. As it was pointed out in the introduction of this work a significant amount of research has been conduced in recent years toward the development of non-linear theories of 3-D beams. However, many of these theories differ in the order of non-linearity considered in their formulation. For example, second-order displacement field has been used in a formulation of finite element models for 3-D non-linear analysis of beam structures [9,10,22–24,27]. This approximation present several advantages because it simplifies the coupling between the displacement and rotations and so the tangent stiffness matrix (use for the non-linear incremental-iterative analysis) can be simplified. Therefore, this tangent matrix can be decomposed into linear and second-order (non-linear) stiffness matrices. In spite of these advantages, second-order formulation may produce the loss of some significant terms in the non-linear strains and in the tangent stiffness matrix, thus some inaccurate approximations in the coupling between displacement, rotations and their derivates. The loss of these terms may lead to "self-straining" caused by superimposed rigid-body motions [18,28].

In particular the second-order model was modeled approximating $\cos\phi$ and $\sin\phi$ by $(1-\phi^2/2)$ and ϕ, respectively, in Exp. (4) and conserving non-linear terms up to second-order. Therefore the displacement field yields

$$\begin{aligned} u_x &= u_o - \theta_z\bar{y} - \theta_y\bar{z} + \phi\theta_z z - \phi\theta_y y + \omega[\theta - \tfrac{1}{2}(\theta'_y\theta_z - \theta_y\theta'_z)],\\ u_y &= v - \phi z + \tfrac{1}{2}(-\phi^2 y - \theta_z^2\bar{y} - \theta_z\theta_y\bar{z}),\\ u_z &= w + \phi y + \tfrac{1}{2}(-\phi^2 z - \theta_y^2\bar{z} - \theta_z\theta_y\bar{y}). \end{aligned} \tag{43}$$

Then a second-order formulation, Exp. (43), produces the loss of the terms underline in Exp. (24). These terms correspond to the flexural–torsional coupling in the non-linear strains.

In this example a fixed-end beam subjected to a transverse force P at the middle of the span is considered. The geometrical and material properties are the same as the previous example.

A comparison of the load-twisting curves is shown in Fig. 14, when the load is applied on the top flange, and considering three models: present beam model, second-order beam model and Abaqus's shell model.

The second-order rotation model predicts a stiffer postbuckling behavior, while the present beam model agrees with the behavior predicted by the Abaqus shell element. Besides, the buckling load obtained by means of a second-order approximation is greater ($P_{cr} = 7.71$ MN) than the value obtained with the present non-linear higher-order model ($P_{cr} = 6.8$ MN). On the other hand, the buckling load predicted by the classical theory (linear model) is about 4% smaller ($P_{cr} = 6.56$ MN) than the bifurcation value.

Comparing the beam response for the three last conditions considered, the fixed-end beam has the higher buckling load and the larger postbuckling strength. Opposite behavior is observed for the case of cantilever condition where the postbuckling path is hardly flat.

9. Conclusions

This paper uses a geometrically non-linear beam theory of thin-walled beam to investigate buckling and postbuckling behavior of simply supported, cantilever and fixed-end beams subjected to distributed or concentrated loads. The theory is formulated in the context of large displacements and rotations, through the adoption of a shear deformable displacement field (accounting for bending and warping shear) considering moderate bending rotations and large torsional twist. The beam model is valid for arbitrary cross-sections, either open or closed. Based on the Ritz's method, an algebraic system is obtained and then solved by an incremental Newton–Raphson algorithm. Trigonometric functions and a set of beam characteristic orthogonal polynomials are used to discretize the variational equation.

In the case of simply supported ends a practical general formula was obtained for determining the critical loads of lateral buckling for bi-symmetrical thin-walled beams. This formula takes into account the effects of prebuckling and shear deformation for beams subjected to concentrated end moments, concentrated forces, or uniformly distributed loads.

From the numerical examples studied, it is concluded the beam formulation proposed in this paper predict correctly the 3-D non-linear elastic response of thin-walled beams. The postbuckling behavior obtained with the present model is, in general, in good agreement with those obtained with a shell finite element model using Abaqus. The actual load-carrying capacity of elastic beams can be established only by using a non-linear buckling analysis. Based on the numerical results, the following conclusions are made:

- In the case of lateral load, the buckling loads obtained from the classical linear theory are very conservative. So, the influence of the in-plane prebuckling deformations in the determination of critical loads is quite significant in some cases. This effect depends mainly on the relation between the bending stiffnesses, EI_z and EI_y.
- The postbuckling curves of the beam showed a stable and symmetric behavior in all the cases analyzed.
- The bifurcation values, observed in the postbuckling figures, agree with the buckling load computed from the tangential stiffness matrix and with the closed-form solution presented by the authors, for a simply supported beam.
- The prebuckling, buckling and postbuckling behavior is highly dependent of the load height parameter. A stiffer behavior is found when the load is applied on the lowest position (bottom flange). The margins of postbuckling strength are larger for this last load condition.
- The shear deformation effect has been investigated, showing a significant influence for short beams. The shear deformation may significantly reduce the buckling loads and the values of the equilibrium path (postbuckling).
- Finally, the second-order model based on moderate rotations overestimates both the values of critical load and the postbuckling strength, compared with those computed from the present model.

Acknowledgments

The present study was sponsored by Secretaría de Ciencia y Tecnología, Universidad Tecnológica Nacional, and by CONICET.

Appendix

The constitutive law for a bi-symmetric beam is defined in the following form:

$$\{f_g\} = [K]\{\chi\}, \tag{A.1}$$

$$\{f_g\} = [N \;\; M_y \;\; M_z \;\; B \;\; Q_y \;\; Q_z \;\; T_w \;\; T_{sv} \;\; B_1 \;\; P_{yy} \;\; P_{zz} \;\; P_{yz}]^T, \tag{A.2}$$

$$\{\chi\} = [ED_1 \;\; ED_2 \;\; ED_3 \;\; ED_4 \;\; ED_5 \;\; ED_6 \;\; ED_7 \;\; ED_8 \;\; ED_9 \;\; ED_{10} \;\; ED_{11} \;\; ED_{12}]^T, \tag{A.3}$$

where $\{f_g\}$ is the vector of generalized forces, $\{\chi\}$ is the vector of the generalized strains and $[K]$ is a symmetric matrix (12×12) where the stiffnesses corresponding to the higher-order terms B_1, P_{yy}, P_{zz} and P_{yz} are given by the following contour

integrals:

$$K = \begin{bmatrix} \mathrm{EA} & 0 & 0 & 0 & 0 & 0 & 0 & 0 & \mathrm{Ek}_{1,9} & \mathrm{Ek}_{1,10} & \mathrm{Ek}_{1,11} & \mathrm{Ek}_{1,12} \\ & \mathrm{EI}_y & 0 & 0 & 0 & 0 & 0 & 0 & \mathrm{Ek}_{2,9} & \mathrm{Ek}_{2,10} & \mathrm{Ek}_{2,11} & \mathrm{Ek}_{2,12} \\ & & \mathrm{EI}_z & 0 & 0 & 0 & 0 & 0 & \mathrm{Ek}_{3,9} & \mathrm{Ek}_{3,10} & \mathrm{Ek}_{3,11} & \mathrm{Ek}_{3,12} \\ & & & \mathrm{EC}_w & 0 & 0 & 0 & 0 & \mathrm{Ek}_{4,9} & \mathrm{Ek}_{4,10} & \mathrm{Ek}_{4,11} & \mathrm{Ek}_{4,12} \\ & & & & \mathrm{GS}_y & \mathrm{GS}_{yz} & \mathrm{GS}_{yw} & 0 & 0 & 0 & 0 & 0 \\ & & & & & \mathrm{GS}_z & \mathrm{GS}_{zw} & 0 & 0 & 0 & 0 & 0 \\ & & & & & & \mathrm{GS}_w & 0 & 0 & 0 & 0 & 0 \\ & & & & & & & \mathrm{GJ} & 0 & 0 & 0 & 0 \\ & & \mathrm{Sym} & & & & & & \mathrm{EI}_R & \mathrm{Ek}_{9,10} & \mathrm{Ek}_{9,11} & 0 \\ & & & & & & & & & \mathrm{Ek}_{10,10} & \mathrm{Ek}_{10,11} & 0 \\ & & & & & & & & & & \mathrm{Ek}_{11,11} & 0 \\ & & & & & & & & & & & \mathrm{Ek}_{12,12} \end{bmatrix}, \tag{A.4}$$

where

$$A = \int \mathrm{d}A,$$

$$I_y = \int Z^2 \,\mathrm{d}A,$$

$$I_z = \int Y^2 \,\mathrm{d}A,$$

$$C_w = \int \omega_p^2 \,\mathrm{d}A,$$

$$S_y = \int Y'^2 \,\mathrm{d}A,$$

$$S_z = \int Z'^2 \,\mathrm{d}A,$$

$$S_w = \int (r-\psi)^2 \,\mathrm{d}A,$$

$$S_{yz} = \int Y'Z' \,\mathrm{d}A,$$

$$S_{yw} = \int Y'(r-\psi) \,\mathrm{d}A,$$

$$S_{zw} = \int Z'(r-\psi) \,\mathrm{d}A,$$

$$J = 4\int \mathrm{d}A,$$

$$I_R = \int (Y^2+Z^2)^2 \,\mathrm{d}A,$$

$$k_{1,9} = \int (Y^2+Z^2) \,\mathrm{d}A,$$

$$k_{1,10} = \int \bar{Z}^2 \,\mathrm{d}A,$$

$$k_{1,11} = \int \bar{Y}^2 \,\mathrm{d}A,$$

$$
\begin{aligned}
k_{1,12} &= \int \bar{Y}\bar{Z}\,\mathrm{d}A,\\
k_{2,9} &= \int \bar{Z}(Y^2+Z^2)\,\mathrm{d}A,\\
k_{2,10} &= \int \bar{Z}^3\,\mathrm{d}A,\\
k_{2,11} &= \int \bar{Y}^2\bar{Z}\,\mathrm{d}A,\\
k_{2,12} &= \int \bar{Y}\bar{Z}^2\,\mathrm{d}A,\\
k_{3,9} &= \int \bar{Y}(Y^2+Z^2)\,\mathrm{d}A,\\
k_{3,10} &= \int \bar{Y}\bar{Z}\,\mathrm{d}A,\\
k_{3,11} &= \int \bar{Y}^3\,\mathrm{d}A,\\
k_{3,12} &= \int \bar{Y}^2\bar{Z}\,\mathrm{d}A,\\
k_{4,9} &= \int \omega_p(Y^2+Z^2)\,\mathrm{d}A,\\
k_{4,10} &= \int \omega_p\bar{Z}^2\,\mathrm{d}A,\\
k_{4,11} &= \int \omega_p\bar{Y}\,\mathrm{d}A,\\
k_{4,12} &= \int \bar{Y}\omega_p\bar{Z}\,\mathrm{d}A,\\
I_R &= \int (Y^2+Z^2)^2\,\mathrm{d}A,\\
k_{9,10} &= \int (Y^2+Z^2)\bar{Z}^2\,\mathrm{d}A,\\
k_{9,11} &= \int (Y^2+Z^2)\bar{Y}^2\,\mathrm{d}A,\\
k_{9,12} &= \int (Y^2+Z^2)\bar{Y}\bar{Z}\,\mathrm{d}A,\\
k_{10,10} &= \int \bar{Z}^4\,\mathrm{d}A,\\
k_{10,11} &= \int \bar{Z}^2\bar{Y}^2\,\mathrm{d}A,\\
k_{10,12} &= \int \bar{Z}^3\bar{Y}\,\mathrm{d}A,\\
k_{11,11} &= \int \bar{Y}^4\,\mathrm{d}A,\\
k_{11,12} &= \int \bar{Y}^3\bar{Z}\,\mathrm{d}A,\\
k_{12,12} &= \int \bar{Z}^2\bar{Y}^2\,\mathrm{d}A.
\end{aligned}
\tag{A.5}
$$

References

[1] V.Z. Vlasov, Thin Walled Elastic Beams, Israel Program for Scientific Translation, Jerusalem, 1961.
[2] S.P. Timoshenko, J.M. Gere, Theory of Elastic Stability, McGraw-Hill, New York, 1961.
[3] R.S. Barsoum, R.H. Gallagher, Finite element analysis of torsional and torsional–flexural stability problems, Int. J. Numer. Methods Eng. 2 (1970) 335–352.
[4] S.T. Woolcock, A.M. Trahair, Post-buckling behavior of determinate beams, J. Eng. Mech. Div. ASCE 100 (1974) 151–171.
[5] Z.P. Bazant, M. El Nimeiri, Large-deflection spatial buckling of thin walled beams and frames, J. Eng. Mech. Div. ASCE 99 (1973) 1259–1281.
[6] K.J. Bathe, S. Bolourchi, Large displacement analysis of three-dimensional beam structures, Int. J. Numer. Methods Eng. 14 (1979) 961–986.
[7] Y.B. Yang, W. McGuire, Stiffness matrix for geometric non-linear analysis, J. Struct. Eng. 112 (1986) 853–877.
[8] A. Hasegawa, K.K. Liyanage, F. Nishino, Spatial instability and non-linear finite displacement analysis of thin-walled members and frames, J. Fac. Eng. Univ. Tokyo 38 (1986) 19–78.
[9] S. Kitipornchai, S.L. Chan, Stability and non-linear finite element analysis, in: J.W. Bull (Ed.), Finite Element Applications to Thin-Walled Structures, Elsevier Applied Science, London, 1990, pp. 89–130.
[10] H. Chen, G.E. Blandford, Thin-walled space frames. II: algorithmic details and applications, J. Struct. Eng. ASCE 117 (1991) 2521–2539.
[11] K.M. Hsiao, W.Y. Lin, A co-rotational finite element formulation for buckling and postbuckling analysis of spatial beams, Comput. Methods Appl. Mech. Eng. 188 (2000) 567–594.
[12] K.M. Hsiao, W.Y. Lin, A co-rotational formulation for thin-walled beams with monosymmetric open section, Comput. Methods Appl. Mech. Eng. 190 (2000) 1163–1185.
[13] W.Y. Lin, K.M. Hsiao, Co-rotational formulation for geometric non-linear analysis of doubly-symmetric thin-walled beams, Comput. Methods Appl. Mech. Eng. 190 (2001) 6023–6052.
[14] A. Grimaldi, M. Pignataro, Post-buckling behavior of thin-walled open cross-section compression members, J. Struct. Mech. 7 (1979) 143–159.
[15] A.N. Kounadis, G.I. Ioannidis, Lateral post-buckling analysis of beam columns, J. Eng. Mech. ASCE 120 (1994) 695–706.
[16] G.I. Ioannidis, A.N. Kounadis, Lateral post-buckling analysis of monosymmetric I-beams under uniform bending, J. Constr. Steel Res. 30 (1994) 1–12.
[17] F. Mohri, L. Azrar, M. Potier-Ferry, Lateral post-buckling analysis of thin-walled open sections beams, Thin Walled Struct. 40 (2002) 1013–1036.
[18] Y.L. Pi, M.A. Bradford, Effects of approximations in analysis of beams of open thin-walled cross-section—part II: 3-D non-linear behaviour, Int. J. Numer. Methods Eng. 51 (2001) 773–790.
[19] Y.L. Pi, M.A. Bradford, Elastic flexural–torsional buckling of continuously restrained arches, Int. J. Solids Struct. 39 (2002) 2299–2322.
[20] Y.L. Pi, M.A. Bradford, Effects of prebuckling deformations on the elastic flexural–torsional buckling of laterally fixed arches, Int. J. Mech. Sci. 46 (2004) 321–342.
[21] Y.L. Pi, M.A. Bradford, F. Tin-Loi, Flexural–torsional buckling of shallow arches with open thin-walled section under uniform radial loads, Thin-Walled Struct. 45 (2007) 352–362.
[22] M.Y. Kim, S.P. Chang, H.G. Park, Spatial postbuckling analysis of nonsymmetric thin-walled frames. I: theoretical considerations based on semitangential property, J. Eng. Mech. 127 (2001) 769–778.
[23] M.Y. Kim, S.P. Chang, S.B. Kim, Spatial postbuckling analysis of nonsymmetric thin-walled frames. II: geometrically non-linear FE procedures, J. Eng. Mech. 127 (2001) 779–790.
[24] S.B. Kim, M.Y. Kim, Improved formulation for spatial stability and free vibration of thin-walled tapered beams and space frames, Eng. Struct. 22 (2000) 446–458.
[25] S.P. Machado, V.H. Cortínez, Lateral buckling of thin walled composite bisymmetric beams with prebuckling and shear deformation, Eng. Struct. 27 (2005) 1185–1196.
[26] S.P. Machado, V.H. Cortínez, Non-linear model for stability of thin walled composite beams with shear deformation, Thin Walled Struct. 43 (2005) 1615–1645.
[27] F. Fraternali, L. Feo, On a moderate rotation theory of thin-walled composite beams, Compos. Part B Eng. 31 (2002) 141–158.
[28] J.C. Simo, L. Vu-Quoc, The role of non-linear theory in transient dynamic analysis of flexible structures, J. Sound Vib. 119 (1987) 487–508.
[29] J.H. Argyris, An excursion into large rotations, Comput. Methods Appl. Mech. Eng. 32 (1982) 85–155.
[30] V.H. Cortínez, M.T. Piovan, Vibration and buckling of composite thin-walled beams with shear deformability, J. Sound Vib. 258 (2002) 701–723.
[31] S. Krenk, O. Gunneskov, Statics of thin-walled pretwisted beams, Int. J. Numer. Methods Eng. 17 (1981) 1407–1426.
[32] K. Washizu, Variational Methods in Elasticity and Plasticity, Pergamon Press, Oxford, 1968.
[33] B.B. Bhat, Transverse vibrations of a rotating uniform cantilever beam with tip mass as predicted by using beam characteristic orthogonal polynomials in the Rayleigh–Ritz method, J. Sound Vib. 105 (1986) 199–210.
[34] Z.P. Bazant, L. Cedolin, Stability of Structures: Elastic, Inelastic, Fracture, and Damage Theories, Dover, Mineola, New York, 2003.
[35] Y.L. Pi, N.S. Trahair, Prebuckling deflections and lateral buckling. II: applications, J. Struct. Eng. ASCE 118 (1992) 2967–2985.